Article:

Yao, G orcid.org/0000-0002-3292-2152, Yang, H, Zhao, J et al. (1 more author) (2020) Experimental study on flow and heat transfer enhancement by elastic instability in swirling flow. International Journal of Thermal Sciences, 157. 106504. ISSN 1290-0729

https://doi.org/10.1016/j.ijthermalsci.2020.106504

Experimental Study on Flow and Heat Transfer Enhancement by Elastic Instability in Swirling Flow

Guice Yao [1,2], Haie Yang [2], Jin Zhao [2], Dongsheng Wen [2,1]

[1]The University of Leeds, Leeds, LS2 9JT, United Kingdom

[2]Beihang University, 100191, Beijing, P. R. China

ABSTRACT

Elastic turbulence has shown great potential to improve mixing and heat transfer performance. Most of the studies, however, are focused on the mixing behaviour, heat transfer characteristics induced by elastic turbulence are still not well established. This work investigates systematically the flow and heat transfer performance by elastic turbulence in a swirling flow region. The heat transfer enhancements in the bulk fluid and between the fluid and the wall are characterised by the effective thermal conductivity and the Nusselt number, respectively. The variations of statistical properties, such as probability distribution functions and spectra profiles are analysed for the characterization of elastic turbulence. The results indicate that viscoelastic fluid intensifies the heat transfer performance with gradually increasing swirling velocity, and a six-times enhancement comparing to the Newtonian fluid at the maximum given swirling velocity is obtained. Particularly, the statistical properties imply that the flow is still in the transition regime to elastic turbulence at $Wi = 5.5$.

Keywords: elastic turbulence; convective heat transfer; swirling flow; pure elastic instability

1. Introduction

The rapid developments of highly integrated devices in many industrial areas, such as information computing technology, chemical process intensification, and ultra-high heat flux encountered in aerospace field [1] require efficient heat transfer technologies. An appropriate heat removal is essential to guarantee an equipment or a system working reliably and efficiently. A conventional method to intensify heat transfer is to induce random flow motion by breaking the insulating layer [2-4], which are generally relied on geometrical modifications to perturb flow [5-7]. However, in many practical applications such as microchannel cooling, the Reynolds number is extremely small and the flow is always in the laminar region, where general passive techniques are become ineffective.

One of the proposed approaches for flow intensification at a very low Reynolds number is to use viscoelastic fluids, which are usually formed by adding small amount of high-molecular-weight polymer into a pure Newtonian solvent [8]. This viscoelastic fluid exhibits dramatic flow instability in the presence of elastic nonlinearity, which is characterized by a normalized Weissenberg number, defined as $Wi=\gamma\cdot\lambda$, where γ is the shear rate applied to the flow and λ is the polymer relaxation time. In particular, when the inertial effects are unimportant at vanishing Reynolds number, the viscoelastic fluids are pronounced to induce purely elastic instability at $Wi > 1$ [9-11], and with further increase of the value of Wi, the flow is excited to a so called elastic turbulence regime [12, 13].

The first experiment on elastic turbulence was conducted by Groisman and Steinberg under a von Karman swirling flow configuration between two disks [14]. Three main features were identified in such a turbulence-like flow: pronounced growth of flow resistance, algebraic decay of angular velocity spectra over a wide range of time scales, and orders of magnitude higher mixing performance compared with Newtonian solvent solely, and all are analogous to hydrodynamic turbulence. The elastic turbulence was also observed in Couette-Taylor geometry and curvilinear channels [15, 16]. The sequences of transition profiles from the onset of elastic instability to elastic turbulence regime were subsequently investigated[17]. A key quantitative property for the elastic turbulence is the exponent value of the power-law spectra, which is significantly different from that of the inertial turbulence of -5/3 [18]. A value in the regime of -3 ~ -4.3 can be regarded as a signal of the occurrence of the elastic turbulence [16, 19-21].

Due to the low Reynolds number flow instability, elastic turbulence shows great potential in intensifying the mixing performance [15, 22, 23]. It has been shown that a viscoelastic fluid could achieve four orders of magnitude enhancement in mixing in a swirling flow region between two parallel plates [16]. Similar intensification were also observed for micro/mini channels [24, 25]. This was attributed to an efficient mixing layer induced by polymer relaxation, leading to a fast mass transfer process. Particularly, the elastic turbulence could contribute to the emulsification process between two immiscible liquids [26], which yields to enhanced oil recovery during the stage of polymer flooding [27-29]. In fact, the mixing performance is significantly affected by the onset of elastic instability, which is highly dependent on the rheological properties of polymer solutions and the geometric elements of flow channel. Due to the discrepancy of polymer relaxation time, chain length and molecular weight, different polymers [26, 30] induced different onset values of elastic instability/turbulence, leading to various mixing performance. Flow in serpentine channels [24, 31-34] , porous media [35, 36] and self-designed channel [37-39] has been recently studied and a consecutive curvilinear streamline is regarded as a necessary condition to trigger elastic instabilities. All these studies showed that the elastic turbulence could indeed benefit the mixing performance. The corresponding mixing enhancement was also applied to indicate the existence of the elastic instability or even elastic turbulence.

Theoretically, an irregular flow motion could not only contribute to the mass transfer but also strengthen the process of heat transfer, which was first investigated in two parallel plates by Traore et al [40]. A self-defined “heat intensity”, characterising the bulk effective heat conduction, showed four times higher than that in a pure Newtonian fluid. Besides, a convective heat transfer between the fluid and the wall, which is highly dependent on polymer concentration, was obtained in a millimetre-sized curvilinear channels [41, 42]. An enhancement of 2-4 times, depending on polymer concentration, was achieved. In particular, when the size of curvilinear channel is scaled down to micro-meter size, such an increasement could reach to two orders of magnitude higher [43, 44], which is much higher than previous results. There were a few other experiments [45, 46] conducted to investigate corresponding heat transfer in different geometries, and all showed the capability of elastic turbulence in improving heat transfer performance, though at different levels.

However it needs to be emphasised that heat transfer intensification by elastic turbulence is still not well established and many questions remain The work conducted so far were conducted in different working conditions and various analysis methods were used, which led to different conclusions. For the studies in curvilinear channels, the characterization of elastic turbulence is highly limited , and whether the flow is in the elastic turbulence regime is still debatable. In general a temperature profile comparing to the conduction limit was used to characterize the heat transfer performance in swirling flow [40], and detailed heat transfer characteristics inside the fluid was not revealed In addition, the convective heat transfer between the wall and the swirling fluid has been generally neglected. Addressing these limitations, this work aims to conduct a systematic study to reveal the heat and mass transfer performance of elastic turbulence or instability in a macroscale swirling flow region between two parallel plates. Both effective thermal conductivity and surface heat transfer Nusselt number were defined to investigate the heat transfer within bulk fluid and between the fluid and the wall, respectively. A statistical analysis and corresponding flow behaviors were also performed to reveal detailed flow dynamics and the relationship between flow and heat transfer.

2. Experimental details

2.1 Experimental system

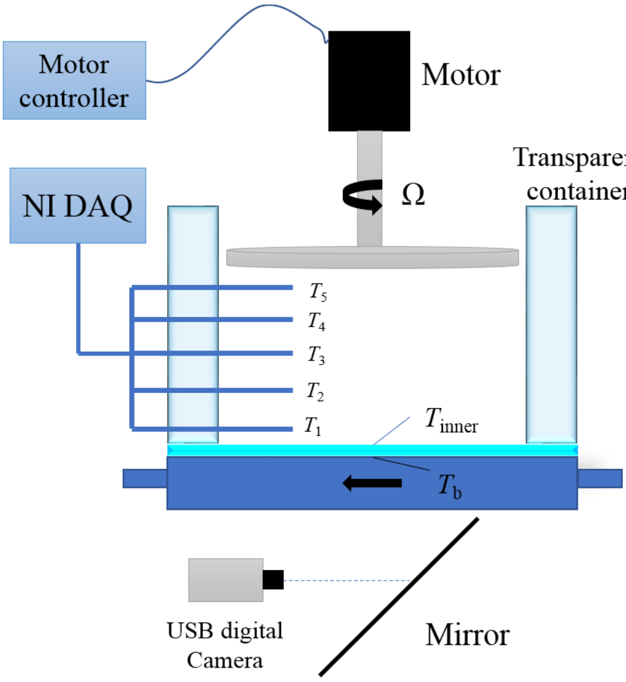

Fig. 1 Schematic view of the experimental setup

The experimental rig that was used to investigate the flow and heat transfer behaviour of viscoelastic fluids in swirling flow is shown in Fig 1. It consists of an acrylic fluid container with inner diameter D_{in}=56 mm and optically transparent walls. The thicknesses of side wall and bottom wall are 10 mm and 5 mm, respectively. The flow was driven by a aluminium rotating round disk with a radius R_d=25 mm mounted on an electric motor, whose controlling precision is up to 0.1 rpm. An insulating cover was placed on the top of the container to prevent the convection of air. The distance between the top disk and the bottom of the fluid container was set at a constant value, H=40 mm, for all experiments. A circulating fluid bath was attached to the bottom of the fluid container and the temperature within which was set at a value of 5 °C to avoid thermal convection inside the bulk flow. To ensure a good repeatability and reproducibility of the experiments, the room temperature was maintained at 23 °C by an air conditioning system.

The temperature distribution into the flow was monitored by an array of five thermocouples (i.e., T_1 to T_5) disposed equidistantly (5mm each point) along the vertical direction z and positioned at the radial position at the half radius of the fluid container. To measure the temperature of the inner wall, a thermocouple was carefully mounted on the bottom and the wire was fixed along the side wall to avoid additional secondary flow. The temperature of the outer wall of the fluid container was averaged based on four thermal couples mounted uniformly along the circular direction in the cooling plate. All thermocouples used in this work were K-type with wire diameter of 0.125 mm, which were calibrated against a mercury thermometer of certified accuracy (± 0.5 °C). The signals of the thermocouples were collected by a National Instrument data acquisition system (NI 9185) and were post-analysed by LabVIEW software.

Besides the temperature measurement, a digital camera and a mirror were coupled together to visualize the flow pattern during the experiments. A mirror tilted by 45° was placed under the fluid container and was used to illuminate the fluid and to relay images of the flow to the camera. It should be noticed that the flow visualization was conducted without circulating fluid bath to avoid the light blockage. . However, the captured images still show significant difference and indicate the occurrence of elastic instability.

2.2 Material properties

Two types of working fluid were used in this study, a Newtonian fluid and a viscous elastic fluid. The Newtonian fluid, regarded as a base fluid, were a 65% sucrose aqueous solution with 1% sodium chloride (referred to “sucrose solution” here after). The viscous elastic fluid was consisted of 200 ppm high-molecular-weight hydrolysed polyacrylamide (HPAM, Mw: 22 M g/mole), 65% sucrose and 1% NaCl solutions (referred to “HPAM solution” here after). The HPAM was supplied by Shandong Tongli Ltd and the other chemicals were obtained from Fisher scientific company. Hereinto, 65% sucrose was conducted as both the base fluid and the solvent of the HPAM solution since it could maximise the relaxation time of the solution and minimise the Reynolds numbers, thereby the flow instabilities were only attributed to the elastic effect rather than the inertial effect.

The viscosities of working fluids against with shear rate at the temperature 15 °C were measured by cone and plate geometry of an MCR 301 rheometer (Anton Paar, Austria) under the stress-controlled mode, as shown in **Fig. 2**. The measurement was conducted with the shear rate ramping from 0.1 to 50 s^{-1}. The viscosity profiles as a function of time at shear rate 0.1 s^{-1} was pre-tested to determine the interval time for the measurement (here 60 s was adopted). The sucrose solution showed a conventional Newtonian behaviour while a shear thinning property was observed for the polymer solution. The values of viscosity at 15 °C was adopted for further calculations for both working fluids since the averaged bulk temperatures were similar and was kept constant at value of 15 °C during the experiments.

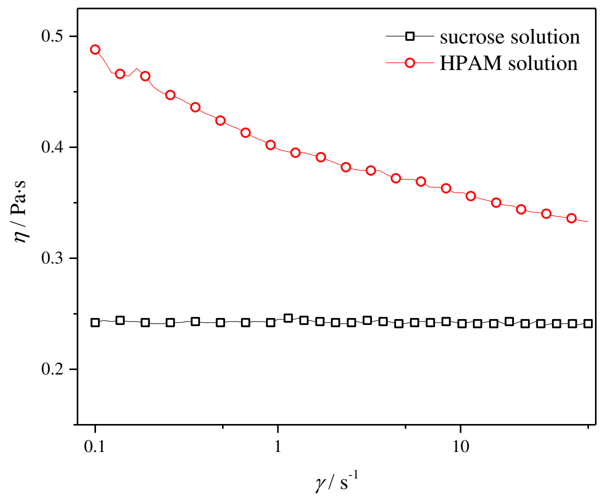

Fig. 2 Viscosity profiles of sucrose solution and HPAM solution

The polymer relaxation time, λ, was measured in the oscillatory test mode at 15 °C with different shear rates. The in-phase and out-of-phase viscosity of polymer solution, η' and η'', respectively, were measured in long series at different angular frequencies ranging from 0.6 to 50 rad·s^{-1}. Same procedures were applied to the pure sucrose solutions and the η_s' and η_s'' were measured as well. The values for the polymer in-phase and out-of-phase viscosity were calculated as $\eta_p'=\eta'-\eta_s'$ and $\eta_p''=\eta''-\eta_s''$, respectively. Then the relaxation time at a specific shear rate was calculated according to equation (1). The oscillatory test profiles and the estimation of relaxation time of HPAM solution at shear rate 1.0 s^{-1} are shown in Fig. 3. The shear dependence of the polymer relaxation time is shown in the inserted figure in the Fig. 3(b) with the scaling $\lambda \propto \gamma^{-\delta}$, where $\delta \approx 0.34$, similar to what was found earlier [11]. With such shear dependent polymer relaxation time is considered, the shearing thinning effect on the onset of elastic instability can be included.

$$\lambda = \lim_{\omega \to 0} \left\{ \frac{1}{\omega} \left[\frac{\eta_P''(\omega)}{\eta_P'(\omega)} \right] \right\} \quad (1)$$

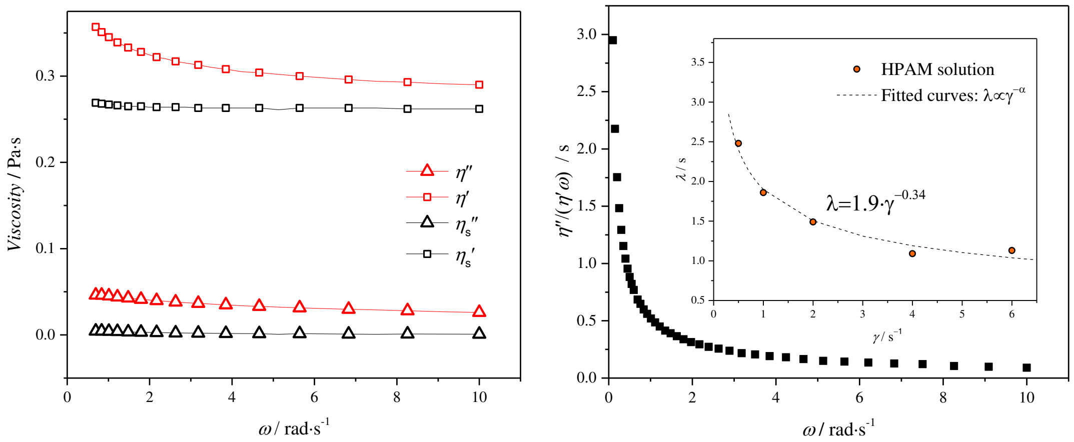

(a) In phase and out of phase viscosity (b) Angular dependence of $\eta''/(\eta'\omega)$

Fig 3 Complex viscosity measurements and relaxation time estimation for sucrose and HPAM solution; the inserted figure in (b) shows the shear rate dependence on relaxation time

Differential scanning calorimetry (DSC) was used to measure the specific heat capacity of working fluids at temperature ranging from 30 to 70 °C as shown in Fig.4. The heat rate for the DSC experiments was set 2 °C/min for all working fluids. The characteristic values of specific heat capacity at 15 °C were then estimated by fitting the experimental data. The addition of polymers to Newtonian solvent does not significantly change the specific heat capacity and the estimated values for both working fluids agreed well with previous studies [41]. Measurement of thermal conductivity was conducted through a probe method (KD2pro thermal properties analyser) at room temperature since an independent relationship between thermal conductivity of sucrose solutions and temperature was identified [43]. The measured thermal conductivity was consistent well with the results of Lee et al. [47], who demonstrated that the addition of polymer up to 10000 ppm to Newtonian solvents did not affect the values of thermal conductivity for these solutions. Therefore, the influence of conduction performance of working fluids on the heat transfer could be eliminated. The representative thermal properties applied in this study are listed in Table 1.

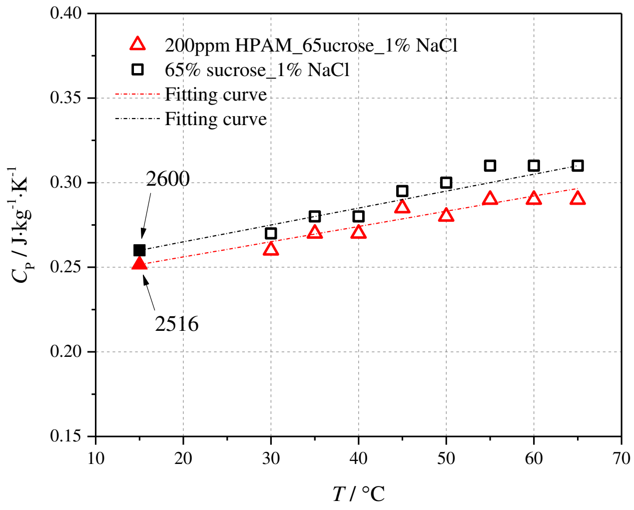

Fig. 4 Measurement of specific heat capacity with various temperature

Table 1 Thermal properties of working fluids

Working solutions	Density ($Kg \cdot m^{-3}$)	Heat specific ($J \cdot K^{-1} \cdot kg^{-1}$)		Thermal conductivity ($W \cdot m^{-1} \cdot K^{-1}$)	
		Measured	Ref.	Measured	Ref.
sucrose	1280	2516	2606 [41]	0.37	0.368 [41]
HPAM	1301	2600	-	0.376	

2.3 Analysis method and error analysis

The heat transfer process during experiments is introduced below. The out wall of the fluid container is set as a constant temperature boundary condition by the cooling circulating system. The side wall can be regarded as a thermal insulation boundary. The amount of heat flux removed by cooling wall can be quantitatively calculated by equation (2).

$$Q = k_{acrylic} \cdot \frac{T_{inner} - T_b}{\delta} \tag{2}$$

Where δ is the thickness of the acrylic wall, T_{inner} and T_{b} are the temperatures of the top and the bottom surface of the wall, respectively; $k_{\text{acrylic}} = 0.18\ W \cdot m^{-1} \cdot K^{-1}$ is the standard thermal conductivity of acrylic materials.

The enhancement of heat transfer by elastic turbulence can be fully quantified via the estimation of the effective thermal conductivity k^* and characteristic Nusselt number Nu^*. The effective conductivity, defined by the ratio of the total measured heat flux and the temperature gradient between the top and the bottom of the fluid container, is adopted to investigate the heat transfer performance within the bulk fluid.

$$k^* = \frac{Q}{\frac{T_5 - T_1}{x_5 - x_1}} \cdot \tag{3}$$

The characteristic Nusselt number, Nu^*, calculated based on the average temperature of the bulk fluid and the inner surface of the wall, represents the ratio of convective heat transfer to purely conductive heat transfer between a moving fluid and a solid surface, defined as:

$$T_{ave} = \frac{T_1 + T_2 + T_3 + T_4 + T_5}{5} \tag{4}$$

$$h^* = \frac{Q}{(T_{ave} - T_{inner})} \tag{5}$$

$$Nu^* = \frac{h^* H}{k} \tag{6}$$

In the present work, the temperature and the depth of the fluids are measured directly by thermocouples and ruler meter. The errors of indirect parameters, for example heat flux, Nusselt number and so on are calculated from the errors of direct measurement parameters using root-sum-square approach as shown in equation (8). The maximum errors of experimental parameters are listed in Table 2.

If $$\chi = S_1^a S_2^b \dots S_N^n \tag{7}$$

Then $$\frac{\delta\chi}{\chi} = \sqrt{\left\{\left(a\frac{\delta S_1}{S_1}\right)^2 + \left(b\frac{\delta S_2}{S_2}\right)^2 + \dots + \left(n\frac{\delta S_N}{S_N}\right)^2\right\}} \tag{8}$$

Table 2 Error estimation of direct and indirect parameters

Parameter	Error (%)	Indirect parameter	Error (%)
T	2.67	Q	5.67
H	0.25	h	6.26
k	5	Nu	8.01
		k^*	6.27

3. Results and discussions

The experiments for both sucrose solution and HPAM solution were conducted by applied rotating angular speed ranging from 0 to 10 rpm. Within the entire range of angular speeds, the Reynolds number of sucrose solution, $Re = \rho\Omega R_d^2/\eta$, was evaluated in the range between 0 and 3.5, which is significantly larger than the largest Re investigated previously with the HPAM solution. Therefore, the comparison between these two working fluids is reasonable to eliminate the influence of inertial effect and the flow instability is solely driven by elastic stresses. Prior to investigating the heat transfer process in a regime of elastic instability, the heat transfer performance based on sucrose Newtonian solution with various angular speed was introduced first as a validation case.

3.1 Heat transfer performance in pure sucrose solution

The time against temperature distribution profiles of the sucrose solution along the vertical direction at various rotating angular speed are shown in Fig. 5(a) (where only temperature profiles at the maximum rotating speed is shown due to the similarity). The initial temperature of working fluid is homogeneous around 21 °C across the whole bulk fluid, followed by a sharp reduction due to the refrigeration system. The temperature near the bottom of the fluid container decreases first and equilibrates at the lowest temperature since the heat is conducted from bottom to top gradually. The measurements for all thermocouples become stable after almost the same time. Even for the maximum applied rotating speed, an obvious separation of temperature layer, which is strongly dependent on the z coordinate, is still observed, indicating a significant inhomogeneous temperature distribution and a conduction like heat transportation. Such behaviours are consistent well with the features of laminar flow. Further analysis was conducted by introducing the reduced temperature θ as defined by equation (9).

$$\theta = \frac{T_0 - T}{T_0 - T_b} \tag{9}$$

Transient measurements of the reduced temperature at maximum applied rotating angular speed are performed in Fig.5(b). The reduced temperature increases as time accumulates with a logarithmic scaling part before reaching a steady plateau state and each transient data is fitted by

$$\theta = A \cdot erfc\left(\frac{B}{\sqrt{t}}\right)^{C} \tag{10}$$

$$B = \frac{z}{(4a)^{\frac{1}{2}}} \tag{11}$$

where *erfc* is the complementary error function, the parameter A describes the equilibrium temperature and B describes the local intensity of the heat transfer process. This function gives exact description for the one-dimensional transient heat transfer in the case of a semi-infinite planar domain with a constant temperature boundary condition when the parameter $C = 1$. By letting C vary as an extra fit parameter, it is reasonable to be applied on finite size conditions. The relationship between fitted coefficients B and the position coordinates z of the thermocouples is shown in Fig.5(c). The thermal diffusivity of the sucrose solution, a, is obtained by linearly fitting the equation (6). The fitted values, as shown in Fig. 5(d), show independence on angular speed and are consistent well with measured values, $a_{meas} = k/(\rho c_p)$, where k is the measured thermal conductivity, ρ is density of the working fluid and c_p is the specific heat capacity of the working fluid, respectively. This reveals a conduction-like heat transfer behaviour occurring within the sucrose solution. This finding corroborates well with a laminar flow behaviour and indicates no inertial instability contributing to the heat transfer intensification. Indeed, CFD simulations by FLUENT 18.1 were conducted to benchmark the experimental results as well. The simulation details are illustrated in the supplementary document. The temperature distribution along the vertical direction is demonstrated in Fig. S5, where a clearly layered temperature profiles was obtained, which is consistent well with the experimental results. What's more, the concomitant *Nu* and k^* calculated based on the simulation results also show a good agreement with experiments as shown in Fig. 8 and 9 in the next section.

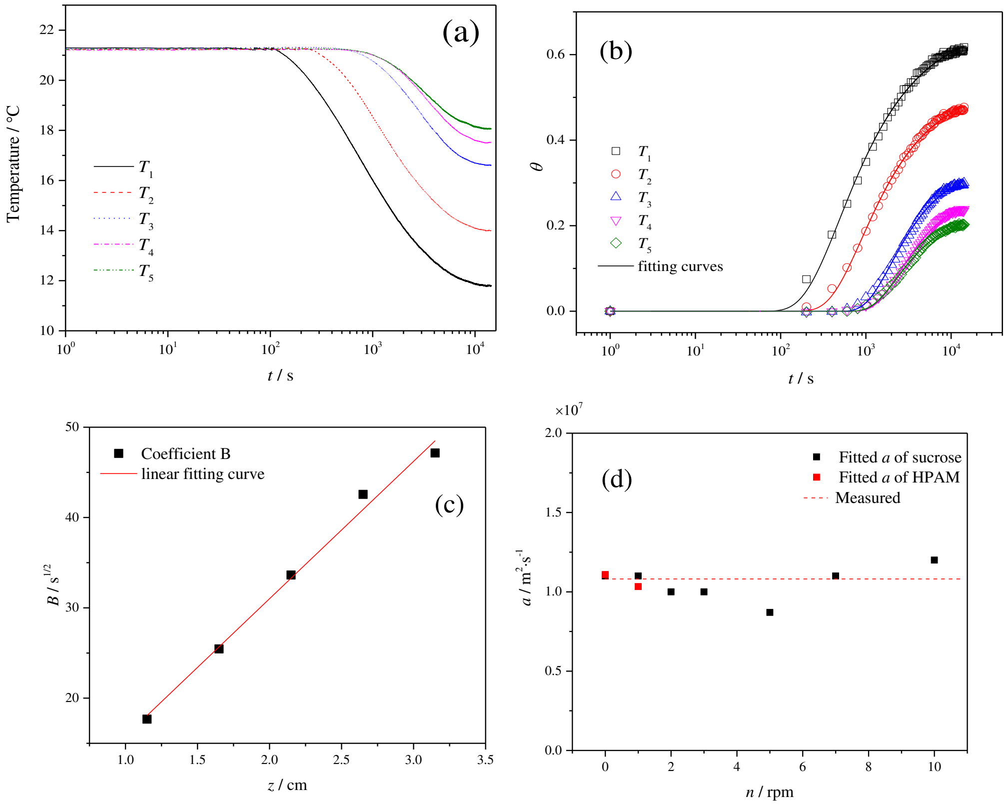

Fig. 5 Temperature distribution profiles for sucrose solution. (a) measured temperature from thermocouples directly at n=10 rpm; (b) reduced temperature distribution at n=10 rpm; (c) thermal diffusivity fitting curve at n=10 rpm (d) variations of thermal diffusivity against different applied rotating speed. The thermal diffusivity for HPAM solution at the two lowest rotating speed are also included

With seeding 1% lighting reflecting flakes into working fluids, the flow visualization was achieved. This particle-filled liquid, so called as Kalliroscope or Rheoscopic liquid, is effective in capturing the flow patterns by reflecting differing intensities of light, making the movement of the streamline visible. Two representative snapshots of the sucrose solution at different rotating speed viewed from below are shown in Fig 6. No obvious irregular flow pattern or vortex is observed even at the largest applied rotating speed. The flow looks quite uniform and is completely laminar, which consistent perfectly with the temperature distribution profiles measured by thermocouples mentioned above. Therefore, it can be concluded that, for pure sucrose solution, the flow stays in laminar regime and the inertial effects could be neglected within the range of rotating angular speed applied during the experiments.

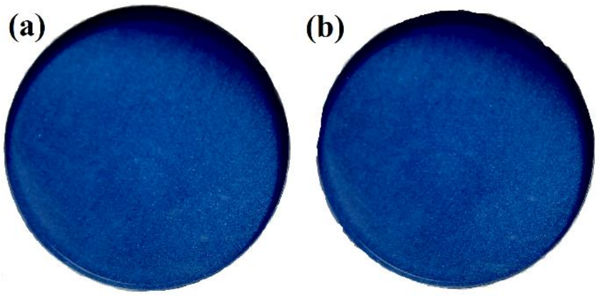

Fig. 6 Flow patterns observed from below at 1 rpm (a) and 10 rpm (b), respectively.

3.2 Heat transfer performance of HPAM solutions

Measurements of the time series of the reduced temperature θ for polymer solutions performed within different rotation speed are presented in Fig S1. Different from the pure sucrose solution, due to the presence of elastic instability, the temperature distributions gradually collapse into a single curve with increasing the rotation speed, indicating the temperature gradually becomes homogenous. It is of note that the slope of such transient temperature variations in this study cannot show the heat transfer performance obviously. Therefore, the convective Nusselt number *Nu* and effective thermal conductivity k^*were adopted to characterize the heat transfer performance.

The equilibrated reduced temperatures are shown in Fig. 7. For the sucrose solution, the equilibrated reduced temperatures for all thermocouples are independent on rotation speed. For the HPAM solution, on the other hand, each reduced temperature decreases slightly at beginning, increases rapidly at a certain value of rotating speed, and collapses into a similar value. This gentle decrease at the beginning is mainly because more heat is transferred into the bulk from the atmosphere due to the instable flow, which makes the temperature near the top region higher. As a result, the temperature even near the bottom increases because of the conductive-like heat transportation. However, such perturbation has slightly effects on the heat transfer performance, which indicates that the temperature distribution profiles cannot represent the heat transfer process sufficiently. The increase after the critical rotating speed is due to that the perturbation moves further in depth which results in lower average temperature. The critical rotating speed varies with the vertical coordinates due to the evolution of the irregular flow. The reduced temperature at the top region is first influenced, followed by the remaining area sequentially from top to bottom.

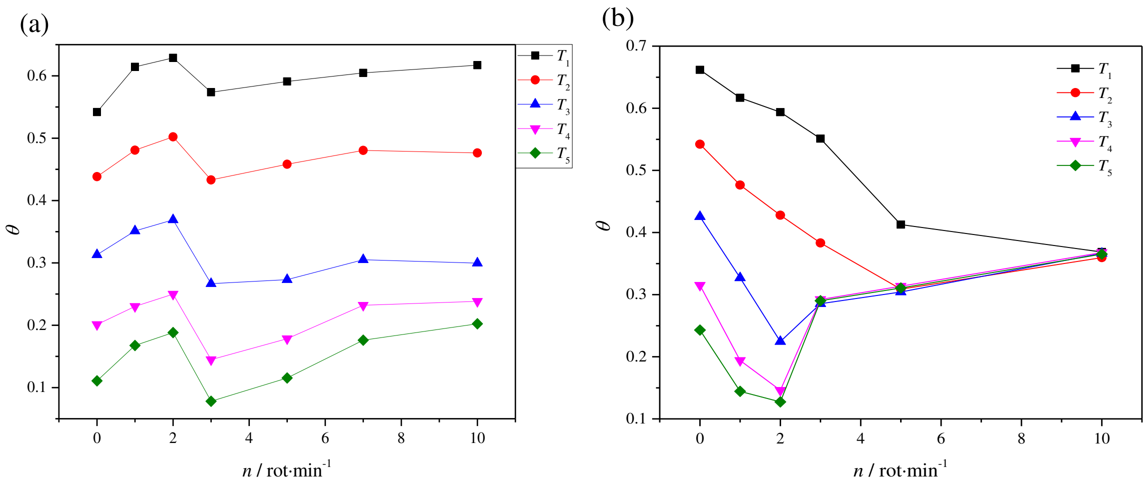

Fig. 7 The equilibrated reduced temperatures for the sucrose solution and the HPAM solution against with rotating speed, (a) the profiles for sucrose solution; (b) the profiles for polymer solution

Based on the equilibrated temperature gradient, the effective thermal conductivities for sucrose and HPAM solutions as a function of *n* and *Wi* are demonstrated in Fig. 8. Due to the sufficiently small temperature difference at larger rotating speed, the estimated effective thermal conductivity is too large to reasonably compare with that for sucrose solution in laminar state. Therefore, only results at the rotating speed lower than 7 rpm are demonstrated. The Weissenberg number was calculated as $Wi = \lambda \gamma^*$, where λ is the characteristic polymer relaxation time, $\lambda = 1.9(\gamma^*)^{-0.34}$, and the γ^* is the modified average shear rate of the bulk fluid. It should be noticed here that, for the case with large gap, the shear rate becomes strong non-homogeneous along the axial direction. In this case, the average shear rate is no longer equal to $2\Omega R/3d$ and should be several times larger. To estimate the real shear rate of the experimental setup, the viscosity of sucrose solution was tested in both standard gap and wide gap geometry (40 mm), as shown in the Fig. S7 in the supplementary documents. It shows that the average shear rate γ^* was proportional to Ω, being $\gamma^*=7.4\Omega R/d$ in this experimental setup.

Both the experimental and modelling effective thermal conductivity of sucrose solution show independent relationship with rotation speed, indicating that there is no chaotic flow behaviour and the flow remains in laminar regime. The only way for heat to transfer from one layer to another is through conduction at the shear layer, which requires more time. The measured effective thermal conductivity agrees well with the simulation results but a bit larger (0.6 and 0.4 $W \cdot m^{-1} \cdot K^{-1}$, respectively), which is mainly ascribed to the position of probe of thermal couples. Due to the soft thermocouple wire, the distance between each probe might be shorter, which results in a larger effective thermal conductivity. This doesn't influence the comparison of Nu since the average temperature was conducted for the calculation of *Nu*.

Unlike sucrose solution, the HPAM solution exhibits a steady period at low rotating speed and a rapid rise starting near n =2 rpm. This tuning point is a reflection of the onset of elastic instability, where the corresponding critical Weissenberg number $Wi_c = 1.8$. The enhancement of the effective thermal conductivity after the occurrence of elastic instability follows an exponential relationship as a function of *Wi*. Compared with the sucrose solution, even the rotating speed is quite low at the value of 7 rpm, where the $Wi = 4.3$ and $Re = 0.8$, respectively, the enhancement of the thermal conductivity of HPAM solution is 22 times higher. It is also interesting to compare the intensification of the heat transport by elastic turbulence with similar experiments performed with Newtonian fluids at large *Re* in the regime of inertial turbulence. Indeed, at the largest applied rotating speed, the effective thermal conductivity is reached to as high as 155 $W \cdot K^{-1} \cdot m^{-1}$. The effective thermal diffusivity $D^* = K^*/\rho c$, is obtained as an approximately value of 0.5 $cm^2 \cdot s^{-1}$, which corresponds to the increase observed in Ref [48] at $Re \approx 1500$.

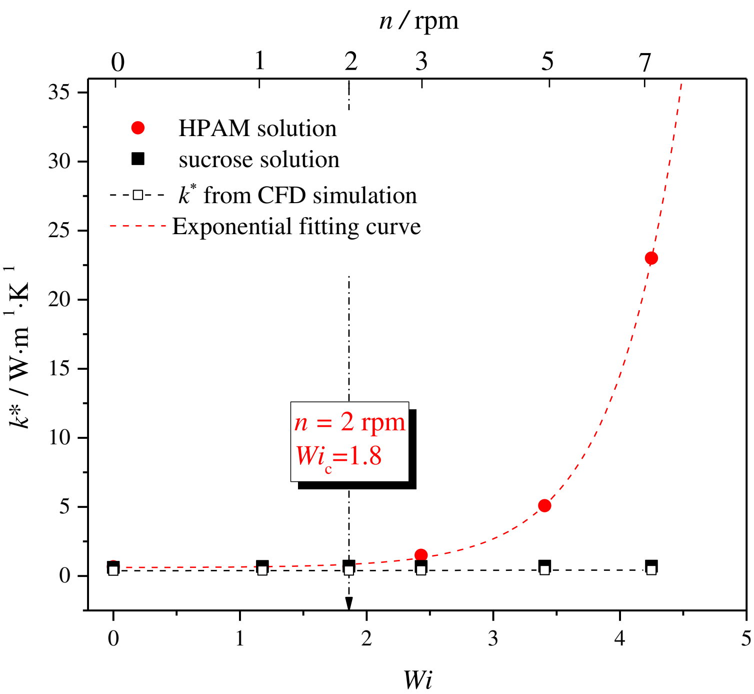

Fig. 8 Dependence of effective thermal conductivity within bulk fluids on degree of rotation for sucrose solution and HPAM solution

The effective thermal conductivity is sensitive with the temperature gradient within the bulk, which is good for capturing the onset condition of the flow instability but fail to characterize the heat transfer performance when the temperature is fully homogeneous. The convective heat transfer *Nu* between the bottom wall and the bulk was conducted instead as shown in Fig 9. As expected, before the elastic instability occurrence, these two fluids exhibit equal heat transfer performance. However, the *Nu* of HPAM solution increases steeply when the rotating speed exceeds the critical value. The flow irregularity moves from one region to another (see from Fig.10), carrying energy between regions, improving the heat transfer performance. After the occurrence of the elastic instability, the *Nu* increases linearly with *Wi*, which is consistent with the results from the investigation of Abed et al [41], where the surface heat transfer for a 100 ppm polymer solution by as much as 240% and by 380% for a 500 pm polymer solution. Indeed, surface convective heat transfer was enhanced dependently by the nonlinear interaction between elastic normal stresses created within the flowing polymer solution and the streamline curvature of the geometry. In the present study, the intensification of the surface heat transfer could reach to 6 times higher, which is in similar degree of heat transfer enhancement with the results from Abed et al and Copeland et al [46] but still seems to be much lower than the enhancement obtained by Li et al [44]. Indeed, the experiments discussed here were conducted in different working conditions. The experimental rig, polymer rheology and even the analysis method were different. It is hard to draw a standard conclusion that how much degree can the elastic turbulence contribute to the heat transfer intensification theoretically since the effects of polymer rheology on the heat transfer are required. However, one can be summarised that elastic turbulence indeed benefit the convective heat transfer performance.

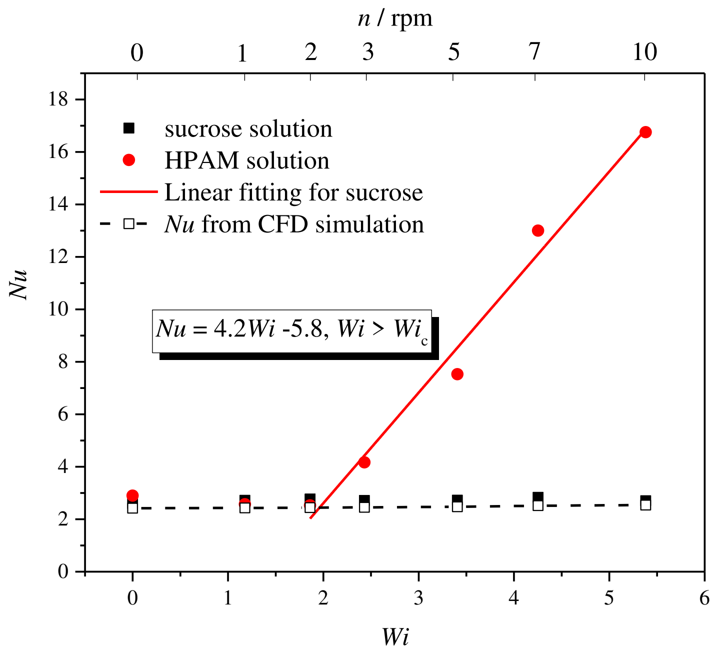

Fig. 9 Dependence of Nusselt number on degree of rotation for sucrose solution and HPAM solution

The corresponding flow behaviours of the HPAM solution captured from the bottom of the fluid container are shown in Fig 10. The patterns of the polymer solution at higher rotating speed look quite irregular and exhibit structures of different sizes. The evolution of these secondary flow patterns could be interpreted by the transition pathway to elastic turbulence in parallel-plate flow observed by Schiamberg et al [17]. The flow sequentially develops as so-called Base state, Stationary ring mode, Competing spirals mode and Multi-spiral chaotic mode, respectively, with increasing the driven shear forces. Compared with the final elastic turbulence mode, the spiral-like flow pattern at maximum applied rotating speed is less intensive, which consistent well with statistical properties discussed in the later section, indicating the flow in still in the transition to elastic turbulence regime. These spiral-like forms are probably imposed by the average of azimuthal flow and circular symmetry of the set-up. Furthermore, a peak point is observed in the middle at stationary ring mode, which corresponds to the centre of a big persistent toroidal vortex and evolves to a spiral vortex latter. Direction of the bursting spiral motion is downwards near the centre and outwards near the bottom, which is attributed to the Weissenberg effect and is opposite to the motion in Newtonian fluids. The visual impression is consistent well with the previous temperature distribution and the existence of the vortexes recommend the elastic turbulence as a potential candidate to enhance heat transfer at least within swirling flow.

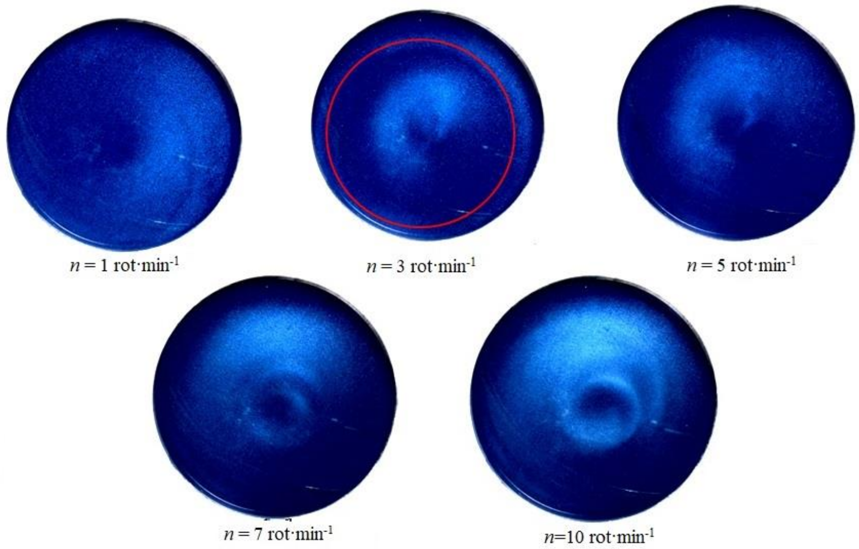

Fig. 10 Snapshots of flow patterns captured from bottom for HPAM solution at different rotating speed

3.3 Statistic properties

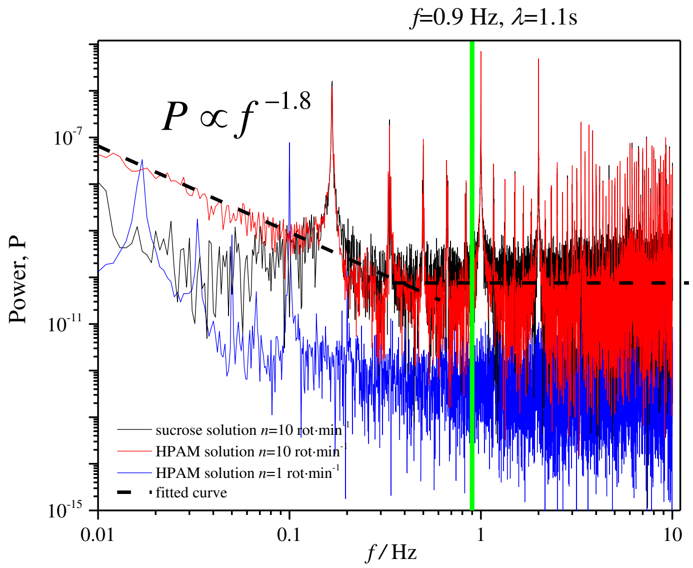

Fig. 11 Power spectra of angular velocity as a function of frequency with various rotating speed

The sharp heat transfer intensification indicates the existence of elastic instability. However, whether this chaotic flow develops into elastic turbulence regime cannot be concluded yet. From the flow patterns captured from below view, the flow seems on its way to elastic turbulence. A main characteristic feature of the elastic turbulence is the power law spectrum of the angular velocity with the exponent value of -3 to -4.3 [16, 21]. In this work, the statistic properties for angular velocity both for sucrose and HPAM solution are shown in Fig. 11. There are some instrumental peaks at f for both curves, which are multiples of the average frequencies of the rotating plate, $\Omega/(2\pi)$. In an elastic turbulence regime, the sharp decay of power spectra of angular velocity occurs when $f > f_{vor}$, where f_{vor} is the main vortex frequency and the frequency $1/\lambda$ corresponds to a low-frequency range (flat dependence rather than power law decay was observed). It can be seen from Fig. 11, there is no clear power-law phenomenon observed after f=$1/\lambda$, which indicates the flow is still not in fully elastic turbulence regime. Such spectra profiles with some distinct peaks and a power-law decay with exponent 1.8 in low frequency domain are quite similar with our previous studies as shown in Fig. S8 in supplementary documents. It is possibly a representative spectra for flow in laminar regime or the beginning of the transition to elastic turbulence, which is indeed directly related to the large-scale vertical flow. In fact, the big toroidal vortex driven by the hoop stress is quite well known to appear in swirling flow of viscoelastic fluids [49] and is the first flow motion above the elastic instability threshold level [16]. What's more it was regarded as the transition to elastic turbulence in the swirling flow between two plates. This is because the toroidal vortex where the liquid and stress tensor imbedded in is chaotically advected and this type of advection can generate variations of stress in a range of smaller scales, which causes small scale fluid motion as a result. As the accumulation of the small-scale motion, the flow transits to the turbulence regime and shows power-law behaviours in high frequency domain, which as described in both our previous works and other's investigations.

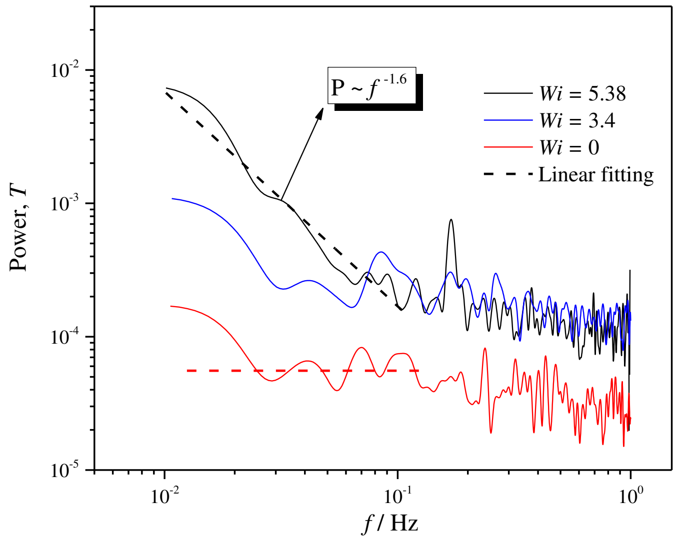

Fig. 12 Power spectra of reduced temperature as a function of frequency with various rotating speeds

The power spectra of the fluctuations of the reduced temperature are shown in Fig. 12. A similar power law dependence of the spectra of temperatures is obtained with exponent of 1.6, which is well consistent with the value of 1.1 observed by Traore et al [40] and Li et al [44]. It should be noticed that such a power law exponent hasn't been identified as a symbol of elastic turbulence since the geometry, materials used in their experiments were different. As we discussed above, the flow in the maximum applied rotating speed is still in the transition region to elastic turbulence. Therefore, such power law dependence only can indicate the existence of elastic instability. Indeed, one of well-known features of temperature in turbulence regime is the near-exponential probability behaviour. Fig. 13(a) shows the probability distribution functions of the fluctuations of reduced temperature at T_4 with various rotating speeds. Both curves are fitted well to the Gaussian equation. However, compared to low rotating speed, with increasing the degree of rotation the PDFs appear to be not far from an exponential function since the tails of the curve seems to be linear and more widely, which is consistent well with the discussion mentioned above that the flow stays in the transition regime rather than elastic turbulence regime. The normalised PDFs for all positions of thermocouples performs similar trends at same applied rotating speed are shown in the Fig. 13(b) and (c). At lower degree of rotation, the flow is quite stable, and the PDF curves collapsed into a single Gaussian curve without any derivations. For higher rotating speed, there are some discrepancies found between each curves, which implies the asymmetric intensity of the flow irregularity. The tails of PDF curves near the position of T_1 thermocouple are not fitted with Gaussian equation and seems to be more irregular.

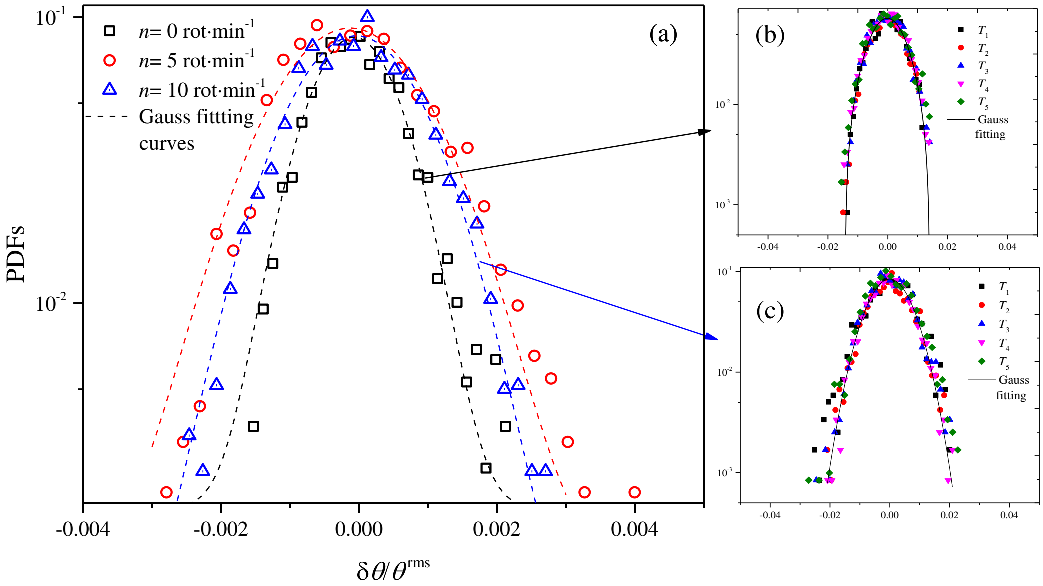

Fig. 13 (a) PDFs of temperature of HPAM solution at T_4 with various rotating speed. (b) and (c) shows the PDFs of temperature at all thermocouples with n=0 rpm and n=10 rpm, respectively

4. Conclusion

Convective heat transfer performance of viscoelastic fluids in a swirling flow between two parallel plates with excitation of pure elastic flow instability was conducted. Based on the experimental results discussed above, the following conclusions can be drawn:

1. Before the occurrence of elastic instability, the HPAM solution exhibits similar heat transfer performance with sucrose, with *Nu* and *k* remain constant . Continually increasing the rotation speed, the elastic instability is induced, which intensifies the heat transfer within bulk fluid and between the wall and the fluid.
2. The critical onset value of elastic instability was determined as *Wi* =1.8 (n= 2 rpm), above which the convective Nu is linearly dependent on the *Wi*. Even at the maximum applied rotating speed, the heat transfer process of sucrose solution is still conduction-like, while in contrast, the HPAM solution could reach to six-times enhancement in heat transfer efficiency.
3. The spiral-like flow behaviour, corresponding with the statistical analysis of temperature and angular velocity, indicates that the flow is still in the transition stage to elastic turbulence over the range of rotating speed applied. The power-law exponent 1.8 at low frequency domain is plausible due to the large scale vortex due to the onset of elastic instability.

Acknowledgments

The work is supported by NSFC under Grants 51876006. The China Scholarship Council is appreciated for sponsoring the PhD project of G.Y.

Conflicts of

The authors declare no competing financial interest.

References

[1] M. Sheikholeslami, M. Gorji-Bandpy, D.D. Ganji, Review of heat transfer enhancement methods: Focus on passive methods using swirl flow devices, Renewable and Sustainable Energy Reviews, 49 (2015) 444-469.

[2] A. Mokrani, C. Castelain, H. Peerhossaini, The effects of chaotic advection on heat transfer, International Journal of Heat and Mass Transfer, 40(13) (1997) 3089-3104.

[3] S.W. Jones, O.M. Thomas, H. Aref, Chaotic advection by laminar flow in a twisted pipe, Journal of Fluid Mechanics, 209 (1989) 335-357.

[4] C. Castelain, A. Mokrani, Y. Le Guer, H. Peerhossaini, Experimental study of chaotic advection regime in a twisted duct flow, European Journal of Mechanics-B/Fluids, 20(2) (2001) 205-232.

[5] A. Dewan, P. Mahanta, K.S. Raju, P.S. Kumar, Review of passive heat transfer augmentation techniques, Proceedings of the Institution of Mechanical Engineers, Part A: Journal of Power and Energy, 218(7) (2004) 509-527.

[6] S. Liu, M. Sakr, A comprehensive review on passive heat transfer enhancements in pipe exchangers, Renewable and sustainable energy reviews, 19 (2013) 64-81.

[7] J. Zhao, S. Huang, L. Gong, Z. Huang, Numerical study and optimizing on micro square pin-fin heat sink for electronic cooling, Applied Thermal Engineering, 93 (2016) 1347-1359.

[8] R.B. Bird, R.C. Armstrong, O. Hassager, C.F. Curtiss, Dynamics of polymeric liquids, Wiley New York, 1977.

[9] S.J. Muller, R.G. Larson, E.S.J.R.A. Shaqfeh, A purely elastic transition in Taylor-Couette flow, 28(6) (1989) 499-503.

[10] R.G. Larson, E.S. Shaqfeh, S.J.J.J.o.F.M. Muller, A purely elastic instability in Taylor–Couette flow, 218 (1990) 573-600.

[11] A. Groisman, V.J.P.o.F. Steinberg, Mechanism of elastic instability in Couette flow of polymer solutions: experiment, 10(10) (1998) 2451-2463.

[12] G. Vinogradov, V.J.K.-Z.u.Z.f.P. Manin, An experimental study of elastic turbulence, 201(2) (1965) 93-98.

[13] R.G.J.N. Larson, Fluid dynamics: turbulence without inertia, 405(6782) (2000) 27.

[14] A. Groisman, V. Steinberg, Elastic turbulence in a polymer solution flow, Nature, 405(6782) (2000) 53-55.

[15] A. Groisman, V.J.N. Steinberg, Efficient mixing at low Reynolds numbers using polymer additives, 410(6831) (2001) 905.

[16] A. Groisman, V. Steinberg, Elastic turbulence in curvilinear flows of polymer solutions, New Journal of Physics, 6(1) (2004) 29.

[17] B.A. Schiamberg, L.T. Shereda, H.U.A. Hu, R.G. Larson, Transitional pathway to elastic turbulence in torsional, parallel-plate flow of a polymer solution, Journal of Fluid Mechanics, 554(-1) (2006) 191.

[18] A.N. Kolmogorov, The local structure of turbulence in incompressible viscous fluid for very large Reynolds numbers, in: Dokl. Akad. Nauk SSSR, 1941, pp. 299-303.

[19] A. Fouxon, V. Lebedev, Spectra of turbulence in dilute polymer solutions, Physics of Fluids, 15(7) (2003) 2060-2072.

[20] T. Burghelea, E. Segre, V. Steinberg, Role of elastic stress in statistical and scaling properties of elastic turbulence, Phys Rev Lett, 96(21) (2006) 214502.

[21] Y. Jun, V. Steinberg, Power and pressure fluctuations in elastic turbulence over a wide range of polymer concentrations, Phys Rev Lett, 102(12) (2009) 124503.

[22] H.Y. Gan, Y.C. Lam, N.-T. Nguyen, Polymer-based device for efficient mixing of viscoelastic fluids, Applied Physics Letters, 88(22) (2006) 224103.

[23] H.Y. Gan, Y.C. Lam, N.T. Nguyen, K.C. Tam, C. Yang, Efficient mixing of viscoelastic fluids in a microchannel at low Reynolds number, Microfluidics and Nanofluidics, 3(1) (2006) 101-108.

[24] T. Burghelea, E. Segre, I. Bar-Joseph, A. Groisman, V. Steinberg, Chaotic flow and efficient mixing in a microchannel with a polymer solution, Phys Rev E Stat Nonlin Soft Matter Phys, 69(6 Pt 2) (2004) 066305.

[25] T. Burghelea, E. Segre, V. Steinberg, Mixing by polymers: experimental test of decay regime of mixing, Phys Rev Lett, 92(16) (2004) 164501.

[26] R.J. Poole, B. Budhiraja, A.R. Cain, P.A. Scott, Emulsification using elastic turbulence, Journal of Non-Newtonian Fluid Mechanics, 177-178 (2012) 15-18.
[27] A. Clarke, A.M. Howe, J. Mitchell, J. Staniland, L. Hawkes, K. Leeper, Mechanism of anomalously increased oil displacement with aqueous viscoelastic polymer solutions, Soft Matter, 11(18) (2015) 3536-3541.
[28] A.M. Howe, A. Clarke, D. Giernalczyk, Flow of concentrated viscoelastic polymer solutions in porous media: effect of M(W) and concentration on elastic turbulence onset in various geometries, Soft Matter, 11(32) (2015) 6419-6431.
[29] J. Mitchell, K. Lyons, A.M. Howe, A. Clarke, Viscoelastic polymer flows and elastic turbulence in three-dimensional porous structures, Soft Matter, 12(2) (2016) 460-468.
[30] N. Latrache, O. Crumeyrolle, I. Mutabazi, Transition to turbulence in a flow of a shear-thinning viscoelastic solution in a Taylor-Couette cell, Phys Rev E Stat Nonlin Soft Matter Phys, 86(5 Pt 2) (2012) 056305.
[31] F.-C. Li, H. Kinoshita, X.-B. Li, M. Oishi, T. Fujii, M. Oshima, Creation of very-low-Reynolds-number chaotic fluid motions in microchannels using viscoelastic surfactant solution, Experimental Thermal and Fluid Science, 34(1) (2010) 20-27.
[32] J. Zilz, R.J. Poole, M.A. Alves, D. Bartolo, B. Levaché, A. Lindner, Geometric scaling of a purely elastic flow instability in serpentine channels, Journal of Fluid Mechanics, 712 (2012) 203-218.
[33] A. Souliès, J. Aubril, C. Castelain, T. Burghelea, Characterisation of elastic turbulence in a serpentine micro-channel, Physics of Fluids, 29(8) (2017).
[34] L. Ducloue, L. Casanellas, S.J. Haward, R.J. Poole, M.A. Alves, S. Lerouge, A.Q. Shen, A.J.a.p.a. Lindner, Secondary flows of viscoelastic fluids in serpentine microchannels, (2018).
[35] C. Scholz, F. Wirner, J.R. Gomez-Solano, C. Bechinger, Enhanced dispersion by elastic turbulence in porous media, EPL (Europhysics Letters), 107(5) (2014) 54003.
[36] D. Kawale, E. Marques, P.L. Zitha, M.T. Kreutzer, W.R. Rossen, P.E. Boukany, Elastic instabilities during the flow of hydrolyzed polyacrylamide solution in porous media: effect of pore-shape and salt, Soft Matter, 13(4) (2017) 765-775.
[37] P. Ligrani, B. Lund, A. Fatemi, Miniature Viscous Disk Pump: Performance Variations From Non-Newtonian Elastic Turbulence, Journal of Fluids Engineering, 139(2) (2016) 021104.
[38] B. Lund, P. Ligrani, M. Brown, DEVELOPMENT AND CONTROL OF ELASTIC TURBULENCE WITHIN A MICRO-SCALE VISCOUS DISC PUMP, Advances and Applications in Fluid Mechanics, 19(3) (2016) 517.
[39] P.C. Sousa, F.T. Pinho, M.A. Alves, Purely-elastic flow instabilities and elastic turbulence in microfluidic cross-slot devices, Soft Matter, 14(8) (2018) 1344-1354.
[40] B. Traore, C. Castelain, T. Burghelea, Efficient heat transfer in a regime of elastic turbulence, Journal of Non-Newtonian Fluid Mechanics, 223 (2015) 62-76.
[41] W.M. Abed, R.D. Whalley, D.J.C. Dennis, R.J. Poole, Experimental investigation of the impact of elastic turbulence on heat transfer in a serpentine channel, Journal of Non-Newtonian Fluid Mechanics, 231 (2016) 68-78.
[42] R. Whalley, W. Abed, D. Dennis, R. Poole, Enhancing heat transfer at the micro-scale using elastic turbulence, Theoretical and Applied Mechanics Letters, 5(3) (2015) 103-106.
[43] D.-Y. Li, X.-B. Li, H.-N. Zhang, F.-C. Li, S.-Z. Qian, S.W. Joo, Measuring heat transfer performance of viscoelastic fluid flow in curved microchannel using Ti–Pt film temperature sensor, Experimental Thermal and Fluid Science, 77 (2016) 226-233.
[44] D.-Y. Li, X.-B. Li, H.-N. Zhang, F.-C. Li, S. Qian, S.W. Joo, Efficient heat transfer enhancement by elastic turbulence with polymer solution in a curved microchannel, Microfluidics and Nanofluidics, 21(1) (2017).
[45] P. Ligrani, D. Copeland, C. Ren, M. Su, M.J.J.o.T. Suzuki, H. Transfer, Heat Transfer Enhancements from Elastic Turbulence Using Sucrose-Based Polymer Solutions, 32(1) (2017) 51-60.
[46] D. Copeland, C. Ren, M. Su, P. Ligrani, Elastic turbulence influences and convective heat transfer within a miniature viscous disk pump, International Journal of Heat and Mass Transfer, 108 (2017) 1764-1774.
[47] W. Lee, Y. Cho, J.J.L.i.H. Hartnett, M. Transfer, Thermal conductivity measurements of non-Newtonian fluids, 8(4) (1981) 255-259.

[48] J.P. Gollub, J. Clarke, M. Gharib, B. Lane, O.J.P.r.l. Mesquita, Fluctuations and transport in a stirred fluid with a mean gradient, 67(25) (1991) 3507.
[49] J.R. Stokes, L.J. Graham, N.J. Lawson, D.V. Boger, Swirling flow of viscoelastic fluids. Part 2. Elastic effects, Journal of Fluid Mechanics, 429 (2001) 117-153.